Theory of control of optomechanical transducers for quantum networks

Theory of control of optomechanical transducers for quantum networks

Fang-Yu Hong,[1] Yang Xiang,[2] W. H. Tang,[1] Zhi-Yan Zhu,[1] Li-zhen Jiang,[3] and Liang-neng Wu[4]

[1]*Department of Physics, Center for Optoelectronics Materials and Devices, Zhejiang Sci-Tech University, Hangzhou, Zhejiang 310018, China*

[2]*School of Physics and Electronics, Henan University, Kaifeng, Henan 475004, China*

[3]*College of Information and Electronic Engineering, Zhejiang Gongshang University, Hangzhou, Zhejiang 310018, China*

[4]*College of Science, China Jiliang University, Hangzhou, Zhejiang 310018, China*

(Received 17 May 2011; published 10 January 2012)

We present a scheme of control for the arbitrary optical interface mediated by a nanoscale mechanical oscillator between flying qubits and optical nonactive solid-state qubits. This quantum interface lays the foundation for many key functions of a quantum network, such as transferring, swapping, and entangling qubits between distant nodes of a quantum network. Numerical simulations of the quantum interface operations show high fidelities and robust tolerance under realistic experimental conditions. Compared with a previous scheme [K. Stannigel *et al.*, Phys. Rev. Lett. **105**, 220501 (2010)], it may significantly increase the speed of state transfer operation of high fidelity.

DOI: 10.1103/PhysRevA.85.012309 PACS number(s): 03.67.Hk, 07.10.Cm, 42.50.Wk

I. INTRODUCTION

Quantum networks comprised of local nodes and quantum channels are of fundamental importance for quantum communication and for scalable and distributed quantum computation [1,2]. Quantum interfaces mapping between optical "flying" qubits and "stationary" qubits are essential elements in a quantum network. Light-matter quantum interface protocols based on cavity-assisted Raman processes have been first described and carried out by atomic systems [3–7]. Because of the striking advances in nanoengineering techniques, solid-state quantum systems have become an extremely promising candidate for quantum information processing. Considering that various solid-state spin, charge, and superconducting qubits do not interact coherently with light, recently Stannigel *et al.* [8] suggested using nanoscale mechanical oscillators (NMO), which can be coherently coupled to light through a microtoroidal cavity to circumvent this problem. However, that scheme employs a time-symmetrical single-photon wave packet and mutually time-reversed operations at two nodes to transfer an unknown qubit state and works under the severe adiabatic condition that the strength of the qubit-resonator coupling is far smaller than the rate with which the mechanical excitations of the optomechanical transducer (OMT) are converted into photons [9–12].

This paper proposes a general control scheme of an OMT-based quantum interface interconverting flying and the aforementioned solid-state qubits. We show that the constraints imposed by the Stannigel scheme can be released, significantly saving physical resources and shortening the operation duration of interconverting flying and local qubits. In this scheme the wave packet of the flying qubit can be arbitrarily specified only if it is sufficiently smooth, the controlling laser fields are determined according to the wave packet of the outgoing or incoming photons in the interface, and the operation of generation and absorption of a photon in quantum channels can be significantly accelerated to within 2μs. This quantum interface can perform many important functions of a quantum network, such as sending and receiving a flying qubit with arbitrary pulse shape and photon number $n(\leqslant 1)$, transferring qubit states from one node to another, and generating entanglement either between flying and stationary qubits or between stationary qubits in two remote nodes.

II. QUANTUM INTERFACE DYNAMICS

The prototype quantum interface consisting of a high-Q microtoroidal resonator, a nanomechanical oscillator of vibration frequency ω_r, an optical waveguide (e.g., a tapered fiber), and a solid-state qubit such as a spin qubit is shown in Fig. 1(a). The qubit states $|g\rangle$ and $|s\rangle$ with an energy difference ω_q are provided by electronic spin or charge degrees of freedom and are coupled together with strength λ by a mechanical normal mode through magnetic [13,14] or electrostatic forces [15,16]. Meanwhile the oscillator is coupled to the tightly confined optical modes of frequency ω_c of the microtoroidal cavity through its evanescent field with enhanced optomechanical coupling strength $G = \alpha a_0(\partial\omega_c/\partial x_0)$ [8,17]. Here α is the mean cavity field amplitude, a_0 is the mechanical zero-point oscillation, and x_0 denotes the mean distance of the mechanical oscillator to the toroid. Since the scattering between two counterpropagating modes can be negligible by positioning the mechanical oscillator tangentially to the optical whispering-gallery-mode trajectory as in Fig. 1(a) [8,17,18], here only a forward-circulating cavity mode is considered, which is coupled to the field in the tapered fiber with a constant $\sqrt{\gamma/2\pi}$ [19]. The optical field in the tapered fiber can be efficiently coupled to the toroidal microcavity mode, which is then coupled back to the forward-propagating field in the fiber with an ideality greater than 99.97%, which is defined as the ratio of the amount of power coupled into the desired mode to that coupled into all modes [20]. A simple Hamiltonian modeling the quantum interface is thus ($\hbar = 1$) [8,17,21]

$$\begin{aligned} H = {} & \frac{1}{2}\omega_q\sigma_z + \omega_r b^\dagger b + \Delta_c c^\dagger c + \int_0^\infty \omega f_\omega^\dagger f_\omega d\omega \\ & + \left(\frac{i}{2}\lambda\sigma_+ b + \text{H.c.}\right) + (iGc^\dagger - iG^* c)(b + b^\dagger) \\ & + \int_0^\infty d\omega \left(i\sqrt{\frac{\gamma}{2\pi}} c f_\omega^\dagger + \text{H.c.}\right), \end{aligned} \tag{1}$$

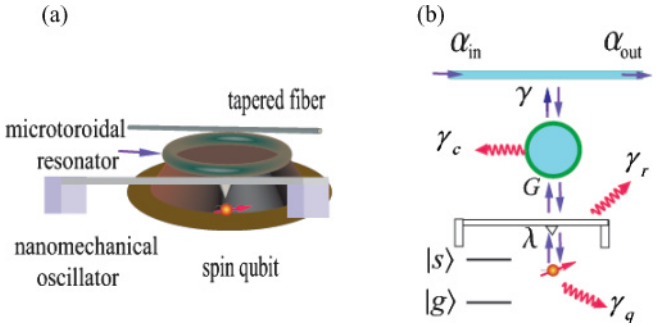

FIG. 1. (Color online) (a) A quantum light-matter interface where quantum information of spin- or charge-based qubits and flying qubits can be interconverted through the aid of an OMT. (b) The interaction between the ingredients of a quantum interface, qubit energy levels, and corresponding decoherence sources.

where σ_z is the Pauli operator, σ_+ and σ_- are the raising and lowering operators for the qubit, respectively, f_ω is the annihilation operator for the mode of frequency ω in the optical channel, and b and c are the annihilation operators for the oscillator and the cavity modes, respectively. The detuning $\Delta_c = \omega_c - \omega_L - 2|G|^2/\omega_r$ and the coupling G can be regulated by the field amplitude and the frequency ω_L of local driving lasers.

Under the rotating-wave approximation (RWA). which holds if $G,\gamma \ll \omega_r + \Delta_c$, the probability of generating more than one exciton is negligible. Hereafter the RWA is assumed. Throughout the whole process of interconverting local and flying qubits in the quantum interface, the state $|g,0,0\rangle|\text{vac}\rangle$ does not evolve into the subspace spanned by basis $|s,0,0\rangle|\text{vac}\rangle$, $|g,1,0\rangle|\text{vac}\rangle$, $|g,0,1\rangle|\text{vac}\rangle$, and $f_\omega^\dagger|g,0,0\rangle|\text{vac}\rangle$, where $|\text{vac}\rangle$ is the vacuum state of the flying qubit, and in notation $|u,j,k\rangle$, $u = g,s$ denotes the stationary qubit states, and j and k denote the number of excitations in the mechanical and cavity modes, respectively. Hence, in the interaction picture the evolution of the system is in the form $|\Psi\rangle = C_g|g,0,0\rangle|\text{vac}\rangle + C_s|\Psi^s(t)\rangle$, where

$$|\Psi^s(t)\rangle = \int_0^\infty d\omega\alpha_\omega f_\omega^\dagger|g,0,0\rangle|\text{vac}\rangle + \beta_s|s,0,0\rangle|\text{vac}\rangle + \beta_r|g,1,0\rangle|\text{vac}\rangle + \beta_c|g,0,1\rangle|\text{vac}\rangle. \quad (2)$$

Under the Hamiltonian given in Eq. (1), within the Weisskopf-Wigner approximation [22] the motion equations for the state amplitudes of the quantum interface system in the interaction picture can be derived as

$$\dot\beta_s = \frac{\lambda}{2}\beta_r e^{-i(\omega_r-\omega_q)t}, \quad (3a)$$

$$\dot\beta_r = -\frac{\lambda^*}{2}\beta_s e^{i(\omega_r-\omega_q)t} - G^*\beta_c e^{i(\omega_r-\Delta_c)t}, \quad (3b)$$

$$\dot\beta_c = G\beta_r e^{-i(\omega_r-\Delta_c)t} - \sqrt{\gamma}\alpha_{\text{in}}(t) - \frac{\gamma}{2}\beta_c \quad (3c)$$

$$= G\beta_r e^{-i(\omega_r-\Delta_c)t} - \sqrt{\gamma}\alpha_{\text{out}}(t) + \frac{\gamma}{2}\beta_c, \quad (3d)$$

where $\alpha_{\text{in}}(t) \equiv \int d\omega\alpha_\omega(t_0)e^{-i(\omega-\Delta_c)t}/\sqrt{2\pi}$ with $t_0 \to -\infty$ and $\alpha_{\text{out}}(t) \equiv \int d\omega\alpha_\omega(t_1)e^{-i(\omega-\Delta_c)t}/\sqrt{2\pi}$ with $t_1 \to +\infty$ are the incoming and outgoing single-photon wave functions in the quantum channel, respectively.

According to Eqs. (3c) and (3d), the solution for β_c is

$$\beta_c(t) = \frac{1}{\sqrt{\gamma}}[\alpha_{\text{out}}(t) - \alpha_{\text{in}}(t)]. \quad (4)$$

From Eq. (3c), the coupling G can be expressed in the form

$$G = \left[\dot\beta_c + \sqrt{\gamma}\alpha_{\text{in}}(t) + \frac{\gamma}{2}\beta_c\right]e^{i(\omega_r-\Delta_c)t}/\beta_r. \quad (5)$$

Substituting Eq. (5) into Eq. (3b), the state amplitudes for the qubit and mechanical mode evolve according to

$$\dot\beta_s = \frac{\lambda}{2}\beta_r e^{-i(\omega_r-\omega_q)t}, \quad (6a)$$

$$\dot\beta_r = -\frac{\lambda^*}{2}\beta_s e^{i(\omega_r-\omega_q)t} - \beta_c\left[\dot\beta_c^* + \sqrt{\gamma}\alpha_{\text{in}}^*(t) + \frac{\gamma}{2}\beta_c^*\right]\Big/\beta_r^*. \quad (6b)$$

From Eqs. (4) and (6) the normalization condition can be derived as follows:

$$\frac{d}{dt}(|\beta_e|^2 + |\beta_r|^2 + |\beta_c|^2) = |\alpha_{\text{in}}(t)|^2 - |\alpha_{\text{out}}(t)|^2. \quad (7)$$

Thus the quantum interface can be designed in this way: first, the wave packets of the outgoing and incoming single photons are arbitrarily assigned only if they are sufficiently smooth; the evolvement of cavity mode $\beta_c(t)$ is then determined according to Eq. (4). Next, the state amplitudes β_s and β_r can, in principal, be solved from Eqs. (6a) and (6b); finally, from Eq. (5) the coupling strength G and therefrom the driving local laser pulse can be set.

This quantum interface can accomplish three types of functions [5]: (I) generating an outgoing photon with an arbitrarily specified wave packet, (II) absorption of an incoming photon with a known wave packet, and (III) absorption of an incoming photon at the same time generating an outgoing photon. Functions (I) and (II) lay the foundation for quantum network operations.

For the sending node of a quantum network, the initial conditions are $\alpha_{\text{in}}(t) = 0$, $\beta_s(t_0) = 1$, $\beta_r(t_0) = 0$, $\beta_c(t_0) = 0$. The outgoing single-photon wave packet can contain an average $\sin^2\theta$ photon with a single-photon wave packet $\tilde\alpha_{\text{out}}(t)$: $\int_{t_0}^{t_1} dt|\alpha_{\text{out}}(t)|^2 = \sin^2\theta\int_{t_0}^{t_1} dt|\tilde\alpha_{\text{out}}(t)|^2 = \sin^2\theta$. At the remote future time $t_1 \to +\infty$, the photon-generation process is completed, and we have $\beta_r(t_1) = 0$, $\beta_c(t_1) = 0$, and $\beta_s(t_1) = \cos\theta e^\phi$ with the phase ϕ determined by Eqs. (6). The most general form of the photon generation process in the quantum interface can be described by Ref. [5]

$$C_g|g,0,0\rangle|\text{vac}\rangle + C_s|s,0,0\rangle|\text{vac}\rangle \xrightarrow{G(t)} C_g|g,0,0\rangle|\text{vac}\rangle + C_s[e^\phi\cos\theta|s,0,0\rangle|\text{vac}\rangle + \sin\theta|g,0,0\rangle|\tilde\alpha_{\text{out}}(t)\rangle]. \quad (8)$$

If $\theta = \pi/2$, Eq. (8) is reduced to

$$C_g|g,0,0\rangle|\text{vac}\rangle + C_s|s,0,0\rangle|\text{vac}\rangle \xrightarrow{G(t)} |g,0,0\rangle[C_g|\text{vac}\rangle + C_s|\tilde\alpha_{\text{out}}(t)\rangle], \quad (9)$$

mapping the stationary qubit state onto the flying qubit. Further, if initially the qubit is in state $|s\rangle$, then this mapping operation can work as the deterministic generation of a single-photon with any desired pulse shape $\tilde\alpha_{\text{out}}(t)$. If $\theta < \pi/2$,

this sending node can also work as generating entanglement between the stationary qubit and the flying qubit:

$$|s,0,0\rangle|\text{vac}\rangle \xrightarrow{G(t)} e^{\phi}\cos\theta|s,0,0\rangle|\text{vac}\rangle + \sin\theta|g,0,0\rangle|\tilde{\alpha}_{\text{out}}(t)\rangle. \tag{10}$$

The receiving process is basically the time reversal of the sending process under the condition $\theta = \pi/2$ [5]. With the qubit initially in state $|g\rangle$ and the incoming flying qubit in state $C_g|\text{vac}\rangle + C_s|\tilde{\alpha}_{\text{in}}(t)\rangle$, the mapping transformation is

$$\begin{aligned}&|g,0,0\rangle(C_g|\text{vac}\rangle + C_s|\tilde{\alpha}_{in}(t)\rangle)\\ &\xrightarrow{G(t)} (C_g|g,0,0\rangle|\text{vac}\rangle + C_s|s,0,0\rangle)|\text{vac}\rangle.\end{aligned} \tag{11}$$

By combining the sending and receiving process, the transfer of a qubit from one node to another can be easily accomplished. When two neighboring nodes carry out state transfer operations followed by receiving state operations at the same time, the two qubits's states are swapped. If $\theta < \pi/2$ for the sending node, the joint operation of the sending and receiving process can generate entanglement between two remote nodes by the transformation

$$|s,g\rangle|\text{vac}\rangle \xrightarrow[G_2(t)]{G_1(t)} (e^{\phi}\cos\theta|s,g\rangle|\text{vac}\rangle + \sin\theta|g,s\rangle)|\text{vac}\rangle. \tag{12}$$

Because of the interaction between the solid-state qubit and the nanomechanical oscillator, Rabi oscillation of the qubit between states $|g\rangle$ and $|s\rangle$ takes place if the state amplitude $\beta_s(t_1) \neq 0$ or $\beta_r(t_1) \neq 0$ when the sending or receiving process is completed. In such cases the coupling strength λ has to be turn off immediately after the corresponding process finishes.

III. NUMERICAL SIMULATION WITH SOURCES OF DECOHERENCE AND DISCUSSION

Now we discuss the effects arising from some inevitable decoherence sources. The equation of motion for the nanomechanical oscillator connected via its support to a thermal bath of temperature T is described by the quantum Langevin equation (QLE)

$$\dot{b} = -i[b,H] - \frac{\gamma_r}{2}b - \sqrt{\gamma_r}\zeta(t), \tag{13}$$

with γ_r being the mechanical decay rate. The mechanical noise operator ζ satisfies $\langle\zeta(t)\zeta(t)^{\dagger}\rangle = (\bar{n}_{th}+1)\delta(t-t')$ and $[\zeta(t),\zeta(t)^{\dagger}] = \delta(t-t')$ with $\bar{n}_{th} = [\exp(\omega_r/k_BT)-1]^{-1}$. Considering $\langle\zeta(t)\rangle = 0$ for a reservoir in thermal equilibrium, from Eq. (13) we have

$$\frac{d}{dt}\langle b\rangle = -i\langle[b,H]\rangle - \frac{\gamma_r}{2}\langle b\rangle = -i\left\langle\left[b, H - i\frac{\gamma_r}{2}b^{\dagger}b\right]\right\rangle, \tag{14}$$

and the mean time development of the number operator has the form [22]

$$\frac{d}{dt}\langle b^{\dagger}b\rangle = -i\langle[b^{\dagger}b,H]\rangle - \gamma_r\langle b^{\dagger}b\rangle + \gamma_r\bar{n}_{th}. \tag{15}$$

For the situation where $k_BT \ll \omega_r, \bar{n}_{th} \to 0$, Eq. (14) reduces to

$$\begin{aligned}\frac{d}{dt}\langle b^{\dagger}b\rangle &= -i\langle[b^{\dagger}b,H]\rangle - \gamma_r\langle b^{\dagger}b\rangle\\ &= -i\left\langle\left[b^{\dagger}b, H - i\frac{\gamma_r}{2}b^{\dagger}b\right]\right\rangle.\end{aligned} \tag{16}$$

Thus the heating of the oscillator from the bath reservoir can be negligible if $k_BT \ll \omega_r$, resulting in an effective Hamiltonian $H_{\text{eff}} = H - i\frac{\gamma_r}{2}b^{\dagger}b$. Taking into account the decoherence sources from the qubit and the cavity by adding two non-Hermitian terms into H_{eff} gives the total effective Hamiltonian,

$$H_{\text{eff}} = H - i\frac{\gamma_q}{2}|s\rangle\langle s| - i\frac{\gamma_r}{2}b^{\dagger}b - i\frac{\gamma_c}{2}c^{\dagger}c, \tag{17}$$

with γ_c being the rate of the intrinsic cavity's photon leakage into free space and γ_q being the rate of qubit spontaneous decay. This Hamiltonian precisely describes the dynamics of the quantum interface under the condition that $k_BT \ll \omega_r$.

Under the action of the effective Hamiltonian (17), the motion Eqs. (3) are replaced by

$$\dot{\beta}_s = \frac{\lambda}{2}\beta_r - \frac{\gamma_q}{2}\beta_s, \tag{18a}$$

$$\dot{\beta}_r = -\frac{\lambda^*}{2}\beta_s - G^*\beta_c e^{i(\omega_r-\Delta_c)t} - \frac{\gamma_r}{2}\beta_r, \tag{18b}$$

$$\dot{\beta}_c = G\beta_r - \sqrt{\gamma}\alpha_{\text{in}}(t) - \left(\frac{\gamma}{2}+\frac{\gamma_c}{2}\right)\beta_c \tag{18c}$$

$$= G\beta_r - \sqrt{\gamma}\alpha_{\text{out}}(t) + \left(\frac{\gamma}{2}-\frac{\gamma_c}{2}\right)\beta_c, \tag{18d}$$

where, for the sake of simplicity, we have assumed the resonance conditions $\omega_r = \omega_q = \Delta_c$. Note that this effective non-Hermitian Hamiltonian approach has been widely used in the literature (see, e.g., [3–5,23–25]).

The qubit-mechanical coupling $\lambda/2\pi \approx 0.59$ MHz for superconducting charge qubits with the decay rate $\gamma_q = 0.02$ MHz is reachable [26,27]. The cavity-fiber coupling is set at a moderate strength $\gamma/2\pi = 3.5$ MHz [5,28], and the intrinsic cavity loss rate is chosen to be $\gamma_c/2\pi = 0.035$ MHz (corresponding to an optical quality factor $Q \sim 10^9$) [29,30]. The mechanical decoherence rate is chosen to be $\gamma_r/2\pi = 0.006$ MHz, corresponding to a mechanical quality factor $Q_m = 8.3\times10^3$ for an oscillator of frequency $\omega_r/2\pi = 50$ MHz [31,32].

Figure 2 shows the simulation result of transfer of an unknown state from node 1 to node 2 under an ideal situation without decoherence sources, assuming the mediator single-photon has a wave packet

$$\begin{aligned}\tilde{\alpha}^{\text{ideal}}_{\text{out1}}(t) &= \tilde{\alpha}^{\text{ideal}}_{\text{in2}}(t) = \tilde{\alpha}^{\text{ideal}}_{a}(t)\\ &= [1-\tanh(\tau t)]\,\text{sech}(0.35\tau t)\\ &\quad + [1+\tanh(\tau t)]\exp(-\tau^2t^2/100),\end{aligned} \tag{19}$$

with normalization understood and $\tau/2\pi = 5$ MHz. The operation durations in the sending and receiving nodes are less than 2 μs. Two control pulses G_1 and G_2 for the sending and receiving processes, respectively, are obtained according to Eq. (5) and are substituted into Eqs. (18), resulting in the fidelity of the generation of a photon with the wave packet

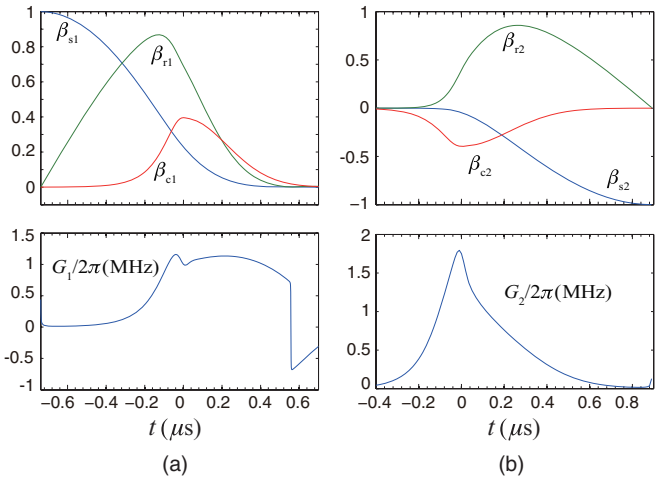

FIG. 2. (Color online) Numerical simulation of state transfer under an ideal situation with the help of a flying qubit of a wave packet $\tilde{\alpha}_a^{\text{ideal}}(t)$. The parameters used are $\gamma/2\pi = 3.5$ MHz, $\lambda/2\pi = 0.59$ MHz. (a) The evolution of state amplitude $\beta_{s1}(t)$, $\beta_{r1}(t)$, and $\beta_{c1}(t)$ and the control pulse $G_1(t)$ for sending node. (b) The same plot for receiving node. Due to $\beta_{s2}(t_1) = -1$, a single qubit transformation $\left[\begin{smallmatrix} 1 & 0 \\ 0 & -1 \end{smallmatrix}\right]$ on qubit 2 is carried out to accomplish the state transfer $C_g|g\rangle_1 + C_s|s\rangle_1 \to C_g|g\rangle_2 + C_s|s\rangle_2$.

$\tilde{\alpha}_{\text{out}}(t_1)$, transferring a target state $|\psi\rangle = (|g\rangle + |s\rangle)/\sqrt{2}$ from one node to another, and generating a target entangled state $|\phi\rangle = (|g\rangle|s\rangle + |s\rangle|g\rangle)/\sqrt{2}$ as

$$F_1 = \left|\langle\tilde{\alpha}_a^{\text{ideal}}|\tilde{\alpha}_{\text{out}}\rangle\right|^2 = 0.9816, \tag{20}$$

$$F_2 = \left|\left[1 + \beta_{s1}^{\text{ideal}}(t_1)\beta_{s1}^*(t_1)\right]/2\right|^2 = 0.9817, \tag{21}$$

$$F_3 = |[\beta_{s1}(t_1) + \beta_{s2}(t_1)]/\sqrt{2}|^2 = 0.9733, \tag{22}$$

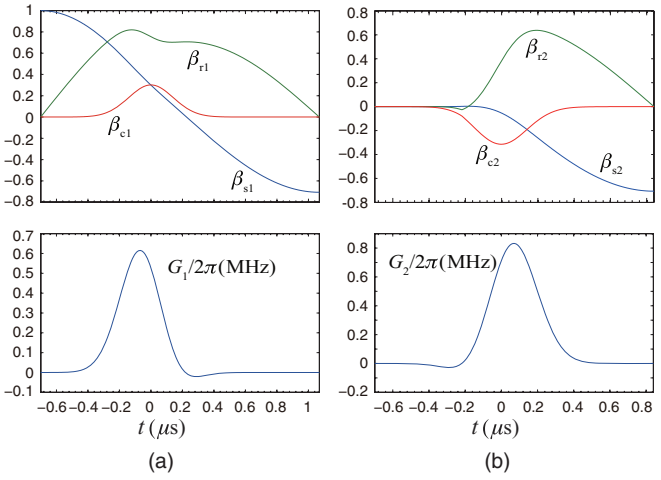

FIG. 3. (Color online) Numerical simulation of distributing entanglement $|\phi\rangle$ between two qubits in the neighboring nodes under an ideal situation, assuming $\tilde{\alpha}_b^{\text{ideal}}(t) = \exp(-(\Gamma t)^2)$ with normalization understood and $\Gamma/2\pi = 0.8$ MHz. Other parameters are as in Fig. 2. (a) The evolution of state amplitude $\beta_{s1}(t)$, $\beta_{r1}(t)$, and $\beta_{c1}(t)$ and the control pulse $G_1(t)$ for sending node. (b) The same plot for receiving node.

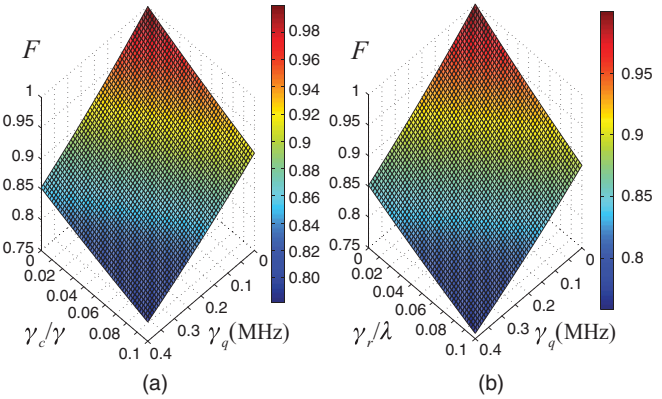

FIG. 4. (Color online) (a) The effect of decoherence sources γ_c and γ_q on the fidelity of transferring state $|\psi\rangle$ from node 1 to node 2 with $\gamma_r = 0$. Other parameters are as in Fig. 2. (b) The same plot for $\gamma_c = 0$ but including the influence of decoherence source γ_r.

respectively, where $\beta_{s1}^{\text{ideal}}(t_1) = 1$. The sharp kink in the control pulse $G_1(t)$ does not cause trouble in experimentally realizing it because the process of sending a single photon is almost complete when the kink takes place at $t_k = 0.55$ μs. To estimate the kink's influence, we perform a numerical simulation with the control pulse $G_1'(t) = 0$ for $t \geqslant t_k$, $G_1'(t) = G_1(t)$ for $t < t_k$, and keeping other parameters unchanged, and we find that the corresponding change in the fidelity of the state transfer F_2 is smaller than 1×10^{-5}.

For comparison, we numerically simulate Eqs. (18) with a wave packet of Gaussian form $\tilde{\alpha}_b^{\text{ideal}}(t) = \exp[-(\Gamma t)^2]$ with normalization understood and $\Gamma/2\pi = 0.8$ MHz. Figure 3 shows the numerical simulation of distributing entanglement between two qubits in the neighboring nodes with a target entanglement state $|\phi\rangle$. When the decoherence sources are included, we have the fidelity of the entanglement distributing operation $F_4 = 9.732$. We find that these two photon wave-packet shapes make very little difference in the effects on the fidelity of the quantum interface operations.

The effects of the decoherence sources on the fidelity of transferring state $|\psi\rangle$ are depicted in Fig. 4. The non-RWA terms in the Hamiltonian (1) contribute decoherence sources to the quantum network tasks by producing more than one exciton in the interface. The effect of these terms scales as γ^2/ω_r^2, G^2/ω_r^2 [18] and is very small for the given parameters and $\omega_r/2\pi = 50$ MHz. Through numerical simulation we find that the probability of generating more than one exciton is estimated to be less than 5×10^{-4} for the given ω_r and the parameters used in Table I. In the above discussion we have assumed that the photon loss in the quantum channel is negligible, which holds for a distance scale of 1 cm [5]. For the situation where photon loss is not negligible one can utilize this scheme with the help of the communication protocols [33,34], which can correct the errors arising from the photon loss. For a distance on the scale of 10^3 km, direct quantum communication is impossible, and we have to resort to quantum repeater protocols [35,36].

According to Eq. (15), one can expect that the influence of the thermal bath on the fidelities of the quantum interface operations scales as $\gamma_r \bar{n}_{th} T_p$ with the pulse length T_p [8]. Here this influence is roughly estimated by inserting an item

TABLE I. Effect of errors in parameters on the fidelity of transferring $|\psi\rangle$ with photon wave-packet shape $\alpha_a^{\text{ideal}}(t)$. The parameters used are $\gamma/2\pi = 3.5$ MHz, $\lambda/2\pi = 0.59$ MHz, $\gamma_c/2\pi = 0.035$ MHz, $\gamma_r/2\pi = 0.006$ MHz, and $\gamma_q = 0.02$ MHz. When the knowledge of the coupling strength is precise, the state transfer fidelity is $F_2 = 0.9817$.

	10% γ error	10% λ error	10% $G_1(t)$ error
Node 1 fidelity	0.9798	0.9695	0.9726
	10% γ error	10% λ error	10% $G_2(t)$ error
Node 2 fidelity	0.9800	0.9692	0.9722

$0.5\gamma_r\bar{n}_{th}$ into the right-hand side of Eq. (18b). The decrease of the state transfer fidelity arising from the thermal bath is roughly estimated to be less than 0.001 for $\gamma_r = 0.01\lambda$, $T = 52.5$ mK, and other parameters used in Table I. Controlling the thermal bath temperature under 52.5 mK is within the reach of current techniques [37–39].

For comparison with the previous scheme, we estimate its performance with the parameters given in the literature [8]. The adiabatic condition requires $\lambda/2\pi \ll \gamma_{op} = \min\{|G|^2\gamma_{\text{tot}}/[\gamma_{\text{tot}}^2 + (\Delta_c - \omega_r)^2], \gamma_{\text{tot}}/2\} \simeq 0.8$ MHz for the median of the coupling strength $G(t) \approx 0.04\omega_r$ shown in Fig. 2 in Ref. [8] and the parameters $(\gamma_{\text{tot}}, \omega_r) = 2\pi \times (5,50)$ MHz for a superconductor charge qubit, where $\gamma_{\text{tot}} = \gamma + \gamma_c$. The literature [8] gives the duration of a state transfer operation in every node as about $25\gamma_{\text{tot}}/\lambda^2$, which equals 3.1 ms for $\lambda/2\pi = 0.1\gamma_{op} = 80$ KHz and is far larger than the lifetime of the charge qubit [27]. Thus we see that the adiabatic condition is very severe, resulting in a very low speed of state transfer operations and the limitation of many possible functions.

In the above numerical simulation, the coupling strength λ, γ, and G are assumed to be exact. However, in real experiment situations, unknown errors in the coupling are inevitable. The effects of unknown errors in the various coupling factors on the quantum state transfer and entanglement generation are estimated and shown in Tables I and II. This quantum control scheme is robust: 10% errors in these coupling strengths decrease the operation quality by less than 2% except in individual cases.

TABLE II. The same as Table I except for generating entangled state $|\phi\rangle$ with photon wave-packet shape $\alpha_b^{\text{ideal}}(t)$. The fidelity of the resulting entangled state is $F_4 = 0.9732$ for the case without errors. Other parameters are as in Table I.

	10% γ error	10% λ error	10% $G_1(t)$ error
Node 1 fidelity	0.9718	0.9057	0.9676
	10% γ error	10% λ error	10% $G_2(t)$ error
Node 2 fidelity	0.9707	0.9613	0.9597

IV. CONCLUSIONS

In summary, we have shown a general control scheme for a quantum light-matter interface mediated by an OMT. This scheme is appropriate for a broad range of solid-state qubits without suitable optical energy transitions. With the requirement of adiabatic conditions and the time-symmetry control pulse removed, it may significantly enhance the speed of quantum network-related operations and expand the capability of the OMT-based quantum interface. It may also find various applications, such as single-photon transistors [25], on-demand single-photon sources [40], and precise measurement of optically nonactive quantum systems [41,42].

ACKNOWLEDGMENTS

This work was supported by the National Natural Science Foundation of China (Grants No. 10874071, No. 50672088, No. 11072218, No. 11005031, and No. 60571029), by the Zhejiang Provincial Natural Science Foundation of China (Grants No. Y6110314 and No. Y6100421), and by the Scientific Research Fund of the Zhejiang Provincial Education Department (Grants No. Y200909693 and No. Y200906669).

[1] J. I. Cirac, A. K. Ekert, S. F. Huelga, and C. Macchiavello, Phys. Rev. A **59**, 4249 (1999).
[2] D. DiVincenzo, Fortschr. Phys. **48**, 771 (2000).
[3] J. I. Cirac, P. Zoller, H. J. Kimble, and H. Mabuchi, Phys. Rev. Lett. **78**, 3221 (1997).
[4] L.-M. Duan, A. Kuzmich, and H. J. Kimble, Phys. Rev. A **67**, 032305 (2003).
[5] W. Yao, R. B. Liu, and L. J. Sham, Phys. Rev. Lett. **95**, 030504 (2005).
[6] H. J. Kimble, Nature (London) **453**, 1023 (2008).
[7] H. P. Specht, Nature (London) **473**, 190 (2011).
[8] K. Stannigel, P. Rabl, A. S. Sorensen, P. Zoller, and M. D. Lukin, Phys. Rev. Lett. **105**, 220501 (2010).
[9] A. Schliesser *et al.*, Nat. Phys. **5**, 509 (2009).
[10] T. J. Kippenberg *et al.*, Science **321**, 1172 (2008).
[11] Q. Lin *et al.*, Nat. Photonics **4**, 236 (2010).
[12] D. Van Thourhout *et al.*, Nat. Photonics **4**, 211 (2010).
[13] P. Rabl, P. Cappellaro, M. V. Gurudev Dutt, L. Jiang, J. R. Maze, and M. D. Lukin, Phys. Rev. B **79**, 041302 (2009).
[14] H. J. Mamin *et al.*, Nat. Nanotechnol. **2**, 301 (2007).
[15] A. D. Armour, M. P. Blencowe, and K. C. Schwab, Phys. Rev. Lett. **88**, 148301 (2002).
[16] M. D. LaHaye *et al.*, Nature (London) **459**, 960 (2009).
[17] G. Anetsberger *et al.*, Nat. Phys. **5**, 909 (2009).
[18] K. Stannigel, P. Rabl, A. S. Sørensen, M. D. Lukin, and P. Zoller, Phys. Rev. A **84**, 042341 (2011).
[19] M. L. Gorodetsky, A. D. Pryamikov, and V. S. Ilchenko, J. Opt. Soc. Am. B **17**, 1051 (2000).
[20] S. M. Spillane, T. J. Kippenberg, O. J. Painter, and K. J. Vahala, Phys. Rev. Lett. **91**, 043902 (2003).
[21] S. Mancini, D. Vitali, and P. Tombesi, Phys. Rev. Lett. **80**, 688 (1998).

[22] M. O. Scully and M. S. Zubairy, *Quantum Optics* (Cambridge University Press, Cambridge, 1997).
[23] M. Roghani, H. Helm, and H.-P. Breuer, Phys. Rev. Lett. **106**, 040502 (2011).
[24] R.- B Liu, W. Yao, and L. J. Sham, Adv. Phys. **59**, 703 (2010).
[25] D. E. Chang *et al.*, Nat. Phys. **3**, 807 (2007).
[26] F. Mallet *et al.*, Nat. Phys. **5**, 791 (2009).
[27] H. Paik *et al.*, Phys. Rev. Lett. **107**, 240501 (2011).
[28] S. M. Spillane, T. J. Kippenberg, K. J. Vahala, K. W. Goh, E. Wilcut, and H. J. Kimble, e-print arXiv:quant-ph/0410218v1.
[29] K. J. Vahala, Nature (London) **424**, 839 (2003).
[30] T. J. Kippenberg *et al.*, Appl. Phys. Lett. **85**, 6113 (2004).
[31] O. Arcizet *et al.*, Nature (London) **444**, 71 (2006).
[32] S. Gigan *et al.*, Nature (London) **444**, 67 (2006).
[33] S. J. van Enk, J. I. Cirac, and P. Zoller, Phys. Rev. Lett. **78**, 4293 (1997).
[34] A. Sørensen and K. Mølmer, Phys. Rev. A **58**, 2745 (1998).
[35] H.-J. Briegel, W. Dür, J. I. Cirac, and P. Zoller, Phys. Rev. Lett. **81**, 5932 (1998).
[36] L.-M. Duan, M. D. Lukin, J. I. Cirac, and P. Zoller, Nature (London) **414**, 413 (2001).
[37] J. D. Teufel, T. Donner, M. A. Castellanos-Beltran, J. W. Harlow, and K. W. Lehnert, Nat. Nanotechnol. **4**, 820 (2009).
[38] A. D. O'Connell *et al.*, Nature (London) **464**, 697 (2010).
[39] M. Poot and H. S. J. van der Zant, e-print arXiv:1106.2060v1.
[40] B. Lounis *et al.*, Rep. Prog. Phys. **68**, 1129 (2005).
[41] D. Rugar *et al.*, Nature (London) **430**, 329 (2004).
[42] K. Jensen *et al.*, Nat. Nanotechnol. **3**, 533 (2008).